P H Y S I C A L   R E V I E W   L E T T E R S

Traveling and Resting Crystals in Active Systems

Andreas M. Menzel[*] and Hartmut Löwen

*Institut für Theoretische Physik II: Weiche Materie, Heinrich-Heine-Universität Düsseldorf,
Universitätsstraße 1, D-40225 Düsseldorf, Germany*
(Received 31 August 2012; revised manuscript received 18 December 2012; published 1 February 2013)

A microscopic field theory for crystallization in active systems is proposed which unifies the phase-field-crystal model of freezing with the Toner—Tu theory for self-propelled particles. A wealth of different active crystalline states are predicted and characterized. In particular, for increasing strength of self-propulsion, a transition from a resting crystal to a traveling crystalline state is found where the particles migrate collectively while keeping their crystalline order. Our predictions, which are verifiable in experiments and in particle-resolved computer simulations, provide a starting point for the design of new active materials.

Self-propelled particles [1] exhibit fascinating collective phenomena like swarming, swirling, and laning which have been intensely explored by theory, simulation, and experiment, for recent reviews, see Refs. [2–4]. In marked contrast to passive particles, self-propelled "active" particles have an internal motor of propulsion, dissipate energy, and are therefore intrinsically in nonequilibrium. Examples of active particles include living systems, like bacteria and microbes [5], as well as man-made microswimmers, catalytically driven colloids [6,7], and granular hoppers [8].

If, at high densities, the particle interaction dominates the propulsion, crystallization in an active system is conceivable. It is expected that such "active crystals" have structural and dynamical properties largely different from equilibrium crystals due to the intrinsic drive. In fact, there is experimental evidence for active crystals, both from observations of hexagonal structures for catalytically-driven colloids [9] and honeycomb-like textures for flagellated marine bacteria [10,11]. Moreover, recent computer simulations have confirmed crystallization [12–15] and proved that melting of active crystals differs from its equilibrium counterpart. However, though field-theoretical modeling of active systems has been widely applied to orientational ordering phenomena [2,16], there is no such theory for translational ordering of active crystals nor has a systematic classification of active crystals been achieved.

Here, we present a microscopic field-theoretical approach to crystallization in active systems and we propose a minimal model which has the necessary ingredients for both, crystallization and activity. In doing so, we combine the phase-field crystal model of freezing [17] with the Toner—Tu model for active systems [18] using the concept of dynamical density functional theory [19,20]. On the one hand, the phase-field-crystal (PFC) model as originally introduced by Elder and co-workers [17,21] describes crystallization of passive particles on microscopic length and diffusive time scales. When brought into connection with dynamical density functional theory [22–25], the PFC

model represents, in principle, a microscopic theory for crystallization, and it has been successfully applied to a plethora of solidification phenomena [17,21,26–30]. On the other hand, Toner and Tu [18] investigated the onset of collective motion in self-propelled systems from a general hydrodynamic point of view. Phenomenological coupling parameters of this model can, in principle, be justified by dynamical density functional theory [31], too, but it does not describe crystallization.

In our PFC model for active systems, we find a wealth of different crystallization phenomena. First, we identify two different types of active crystals which we call "resting" and "traveling" depending on their averaged drift velocity. A resting crystal possesses vanishing net particle flux, whereas a traveling crystal is migrating with a nonzero velocity while keeping its periodicity. Starting from a disordered initial state, a traveling crystal is typically formed by a coarse-graining process of domains. The threshold in the driving strength upon which traveling crystals are formed depends on the spontaneous local orientational order (as prescribed by the coupling parameters of the bare Toner—Tu model): if there is no such order, the threshold is finite, while there is no such threshold in the presence of spontaneous orientational order. We identify a transition from a hexagonal to a rhombic traveling crystal if the drive is increased further as well as resting and traveling lamellar phases with one-dimensional periodic ordering. Finally, the occurrence of honeycomb-like structures can be explained as well within our model. The knowledge of and control over these crystalline states provides an attractive starting point for the design of novel active materials since active crystals possess unique structural, phononic, and rheological properties.

In the following, we first outline our model. Our dynamical equations are for the local one-particle density field $\psi_1(\mathbf{r}, t)$, a conserved scalar order parameter field describing the reduced density modulation around a fixed averaged density $\bar{\psi}$ [17,21], and for a vector field $\mathbf{P}(\mathbf{r}, t)$

characterizing local polar ordering. Activity enters into the equations via a nonzero self-propulsion velocity v_0. In suitably scaled units of time, length, and energy, our basic dynamic equations read

$$\partial_t \psi_1 = \nabla^2 \frac{\delta \mathcal{F}}{\delta \psi_1} - v_0 \nabla \cdot \mathbf{P}, \qquad (1)$$

$$\partial_t \mathbf{P} = \nabla^2 \frac{\delta \mathcal{F}}{\delta \mathbf{P}} - D_r \frac{\delta \mathcal{F}}{\delta \mathbf{P}} - v_0 \nabla \psi_1. \qquad (2)$$

Here, D_r is a rotational diffusion coefficient. $\mathcal{F}$ is a free energy functional of ψ_1 and $\mathbf{P}$, gained from density functional theory. Equations (1) and (2) are consistent with phenomenological symmetry arguments and involve the simplest nontrivial coupling between the two order parameter fields ψ_1 and $\mathbf{P}$. They can also be derived from microscopic dynamical density functional theory [32] within an appropriate gradient and Taylor expansion of the order parameter fields [20,33,34]. In the sequel, we shall consider two spatial dimensions only.

We now further specify the free energy functional $\mathcal{F}$ to $\mathcal{F} = \mathcal{F}_{pfc} + \mathcal{F}_{\mathbf{P}}$ where

$$\mathcal{F}_{pfc} = \int d^2 r \left\{ \frac{1}{2} \psi [\varepsilon + (1 + \nabla^2)^2] \psi + \frac{1}{4} \psi^4 \right\} \qquad (3)$$

is the traditional PFC functional [17,21] describing the tendency of the material to form periodic structures. Here, ε sets the temperature [17,21], and the order parameter ψ corresponds to the total density $\psi = \bar{\psi} + \psi_1$. The polarization-dependent part

$$\mathcal{F}_{\mathbf{P}} = \int d^2 r \left\{ \frac{1}{2} C_1 \mathbf{P}^2 + \frac{1}{4} C_4 (\mathbf{P}^2)^2 \right\} \qquad (4)$$

characterizes local orientational ordering related to the active drive following the approach by Toner and Tu [18] for neglected convection. The two coupling parameters C_1 and C_4 govern the local orientational ordering due to the drive. If $C_1 = C_4 = 0$, only gradients in the density ψ_1 can induce local polar order $\mathbf{P}$ of the active driving. For $C_1 > 0$ ($C_4 = 0$), diffusion tends to reduce the polar order generated by the density gradients. In the third case, $C_1 < 0$ and $C_4 > 0$, a net local driving spontaneously emerges already in the absence of density gradients.

Clearly, on the one hand, for vanishing self-propulsion $v_0 = 0$, Eqs. (1) and (2) decouple and the density equation reduces to the usual phase field crystal model [17,21]. On the other hand, if $\mathcal{F}_{pfc}$ is neglected, the remaining terms are contained in the model by Toner et al. [18,35], except for the higher-order term in $\mathbf{P}$ that contributes to translational diffusion. Summarizing, Eqs. (1)–(4) form a minimal approach to characterize crystallization in actively driven systems.

We numerically determined the phase diagram by scanning the $\bar{\psi}$-ε plane while keeping the parameters C_1, C_4, and v_0 fixed. As for any numerical result reported subsequently, we for each set of parameter values

($\bar{\psi}$, ε, C_1, C_4, v_0) started from random initial conditions and then iterated Eqs. (1)–(4) forward in time. Numerical measurements were carried out after equilibration, and a systematic finite size study was performed to test the validity of our results.

For the decoupled case $v_0 = 0$, the equilibrium phase diagram [21] corresponding to the energy functional Eq. (3) is shown in Fig. 1(a). For nonzero active drive v_0, we will first report on the case $C_1 > 0$.

When we moderately increase v_0 from zero for $C_1 > 0$, the phase boundaries undergo a temperature shift $\Delta \varepsilon$ to lower temperatures. An example is depicted in Fig. 1(b). Comparison to Fig. 1(a) shows that switching on the active drive melts crystals and lamellae close to the liquid phase boundary. The patterns still remain at rest, however. For this case, a linear stability analysis and derived amplitude equations for ψ_1 and $\mathbf{P}$ predict $\Delta \varepsilon \propto v_0^2 / C_1$, which was also verified numerically. In this sense, self-propulsion renormalizes the temperature corresponding to the motion of the individual self-propelled particles when interpreted in terms of a diffusion process [36,37].

We present an example snapshot of the resting crystalline phase in Fig. 2(a). The peaks of the density distribution ψ_1 form a hexagonal lattice as dictated by the PFC energy functional. $\mathbf{P}$ points down the density gradients. Consequently, the polarization field forms "+1"-defects centered at the density peaks. Since $\mathbf{P}$ describes the local direction of active drive, density is convected out of the peaks by the active propulsion v_0. This mechanism counteracts the density diffusion into the peaks described by the PFC energy functional. Therefore, lower temperatures are
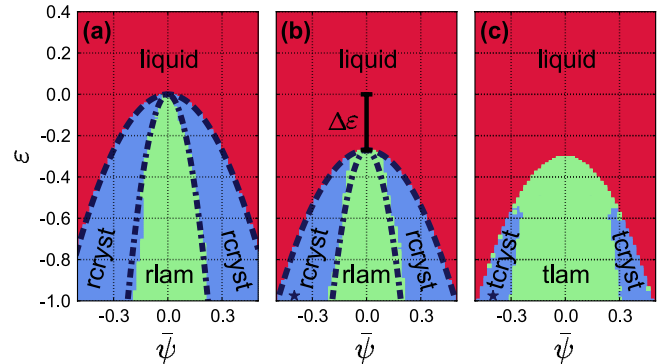
FIG. 1 (color online). Phase diagrams ("rcryst": resting crystals; "rlam": resting lamellae; "tcryst": traveling crystals; "tlam": traveling lamellae). (a) For $C_1 = 0$, $v_0 = 0$ the equilibrium phase field crystal model is recovered. Equilibrium phase boundaries given by the energy functional are indicated for the liquid–hexagonal (dashed line) and hexagonal–lamellar (dash-dotted line) transitions. (b) For $C_1 = 0.2$, $v_0 = 0.35$ the structures are still at rest, but the phase boundaries are shifted by a value $\Delta \varepsilon$. (c) For $C_1 = 0.2$, $v_0 = 0.7$ the structures are traveling and phase boundary lines are omitted for clarity. The black stars in the bottom left of panels (b) and (c) mark the intersection points with the curve in Fig. 3. In all cases $C_4 = 0$, $D_r = 0.5$.
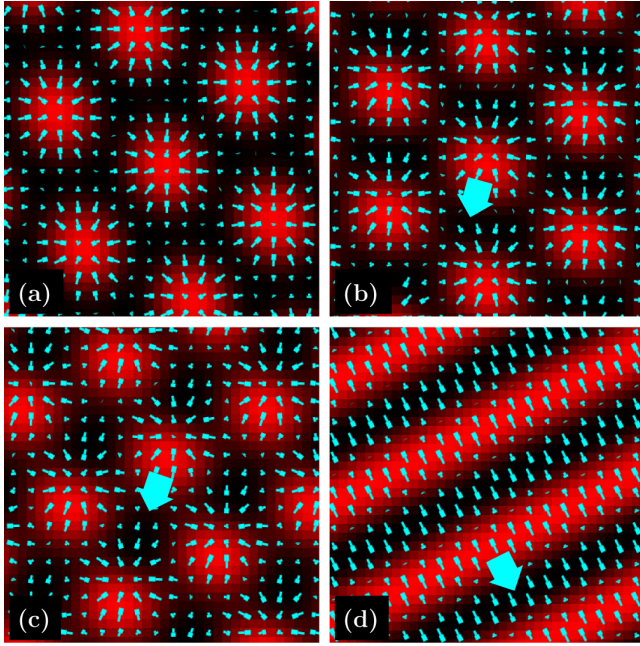
FIG. 2 (color online). Snapshots of the order parameter fields for the different phases observed with increasing active drive v_0 at $(\bar{\psi}, \varepsilon, C_1, C_4) = (-0.4, -0.98, 0.2, 0)$: (a) resting hexagonal, $v_0 = 0.1$, (b) traveling hexagonal, $v_0 = 0.5$, (c) traveling quadratic, $v_0 = 1$, (d) traveling lamellar, $v_0 = 1.9$. Brighter color corresponds to higher densities ψ_1. Thin bright needles illustrate the polarization field **P** pointing from the thick to the thin ends. In panels (b)—(d) the predominant direction of motion is indicated by the bright arrows. Only a fraction of the numerical calculation box is shown.

necessary for the patterns to form in the presence of an active drive, corresponding to the temperature shift $\Delta\varepsilon$ in Fig. 1(b). In the resting crystalline and lamellar case, both tendencies balance each other so that the averaged net particle flux vanishes.

With increasing active drive, the density peaks start to travel above a critical value $v_{0,c}$. Such a state is illustrated in Fig. 2(b). The centers of the density peaks are now shifted with respect to centers of the "$+1$"-defects in the polarization field. This reduced symmetry induces active propulsion: a net orientation of the polarization field emerges when averaged over the area of a single density peak. The consequence is an active convection of each density peak, originating from the PFC density modulation. These results are in agreement with a linear stability analysis of Eqs. (1) and (2) which predicts that propagating modes appear above a threshold value $v_{0,c}$.

With further increasing v_0, the hexagonal pattern is deformed to a rhombic one. In the end, we observe a nearly quadratic structure as depicted in Fig. 2(c). This structural hexagonal–rhombic–quadratic transition appears to be smooth and continuous. Finally, we observe that the traveling crystal can be melted into a traveling lamellar state if v_0 is increased to still higher values. This traveling

crystalline–lamellar transition occurs rather abruptly and is also evident when we compare the two phase diagrams in Figs. 1(b) and 1(c). There, with increasing v_0, the traveling lamellar regions grow into the traveling crystalline regions. An example snapshot of such traveling lamellae is shown in Fig. 2(d).

To quantify the scenario further, we tracked the motion of each density peak. We determined the individual peak velocities $\mathbf{v}_i$, where $i = 1, \ldots, N_p$ and N_p denotes the number of peaks. Samples of up to 1000 density peaks were investigated. The sample-averaged peak velocity magnitude follows as $v_m = \sum_{i=1}^{N_p} \|\mathbf{v}_i\|/N_p$. In addition, we calculated the degree of polar orientational order of the normalized peak velocities $p_v = \|(\sum_{i=1}^{N_p} \mathbf{v}_i/\|\mathbf{v}_i\|)\|/N_p$. This order parameter detects whether the peaks move coherently (collectively) into the same direction.

For $C_1 > 0$, Fig. 3 clearly illustrates the existence of a threshold value $v_{0,c}$ at which propagation starts. As indicated in the inset, we observed a regular *swinging* motion of the hexagonal crystal peaks close to the threshold. With increasing values of active drive, we subsequently find the states illustrated in Figs. 2(a)–2(d). The averaged peak velocity magnitude v_m monotonically increases, except for an abrupt drop at the traveling quadratic–lamellar transition. We can obtain a traveling quadratic crystal
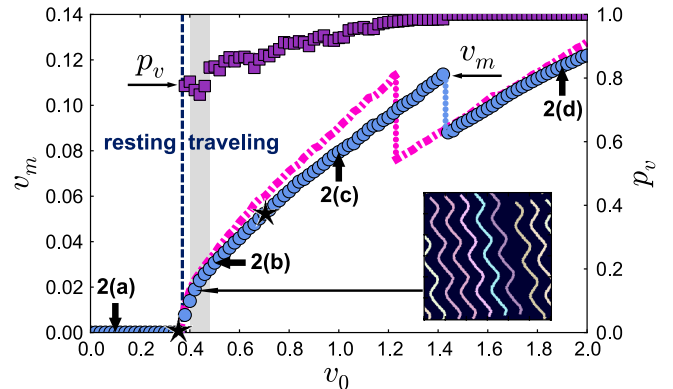
FIG. 3 (color online). Sample-averaged magnitude v_m of the crystal peak velocities (left scale) and polar order parameter p_v of the crystal peak velocity vectors (right scale) as a function of v_0 for $(\bar{\psi}, \varepsilon, C_1, C_4) = (-0.4, -0.98, 0.2, 0)$. At the threshold collective, crystalline motion sets in. Thick arrows mark the positions where the snapshots of Fig. 2 were taken; black stars indicate the intersection points with the phase diagrams in Figs. 1(b) and 1(c). The region above threshold where regular swinging motion could be observed is marked in gray. When a surrounding background fluid can be set into motion, hydrodynamic interactions can increase the nonzero values of v_m (dash-dotted line). Inset: peak trajectories illustrating a state of regular swinging motion in a hexagonal crystal; different colors correspond to different peaks; only trajectories of a horizontal row of density peaks are shown that started at the bottom and were traveling to the top of the picture while tracking was performed.
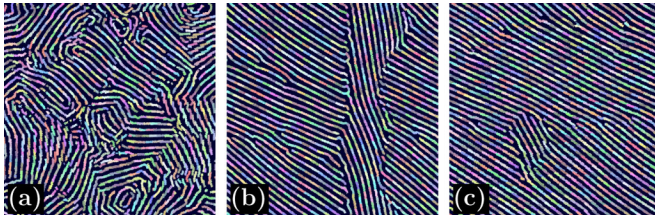
FIG. 4 (color online).   Coarse-graining in a sample of about 1000 traveling density peaks. The sample is in the traveling hexagonal crystalline state. Depicted are instant pieces of all peak trajectories, drawn in different colors. These pieces connect to lines of equal orientation within collectively moving domains. Over time, some domains of equal velocity orientation grow on the cost of others. Parameter values correspond to Fig. 2(b). Dimensionless times [32]: (a) 4500, (b) 50 000, (c) 70 000.

from superimposing perpendicularly oriented traveling lamellae. Their intersections form peaks that travel $\sqrt{2}$ times faster than each single lamella by itself, which explains the magnitude of the drop in the v_m-curve. The lamellae in our case appear from the phase field crystal functional and in this sense are different from the propagating stripe patterns observed before [38]. However, the propagation mechanism is in both cases convection due to self-propulsion [39].

When a surrounding background fluid, up to now considered as overdamped and at rest, can be set into motion, hydrodynamic interactions [40] between the peaks increase the nonzero values of v_m as indicated in Fig. 3 [32]. Furthermore, ordered collective motion generally becomes less stable [41], which here is reflected by an earlier appearance of the lamellar structures. In contrast, the threshold value $v_{0,c}$ remains unaltered.

Furthermore, we observe in Fig. 3 that the polar peak velocity order parameter p_v jumps to a value close to one at the threshold and then further increases. This indicates that after equilibration of the sample the density peaks migrate coherently into the same direction and the crystal travels as a single object. However, at each value of v_0, this collective motion has to first develop from the disordered initial state. The latter process occurs through a coarse-graining dynamics from domains of different directions of collective motion, as qualitatively illustrated in Fig. 4.

Finally, if we set $C_1 < 0$ and $C_4 > 0$, a net polar direction **P** of self-propulsion spontaneously occurs as in the Toner—Tu model [18,35]. For this scenario, we never observed a finite threshold value of v_0. Propagating structures evolved for all tested nonzero values of v_0. Again, a hexagonal–rhombic–quadratic–lamellar transition sequence was observed with increasing v_0. Furthermore, we note that our equations of motion are invariant under the transformation $\bar{\psi} \to -\bar{\psi}$, $\psi_1 \to -\psi_1$, **P** $\to$ −**P**. Consequently, our analysis equally applies for active honeycomb textures when $\bar{\psi} > 0$. Such textures were observed for flagellated marine bacteria [10,11].

In summary, we extended the phase field crystal model [17,21] to active systems by combining it with the approach of Toner *et al.* [18,35]. As a result, the active drive favors the liquid and lamellar states in the PFC phase diagram and induces a wealth of new active crystalline states of hexagonal, honeycomb, rhombic, and quadratic texture. The global motion of all these structured states is either "resting" or "traveling". The transition from "resting" to "traveling" involves a complex intermediate swinging motion. When prepared from an initially disordered state, traveling crystals emerge through coarse-graining from a multidomain texture.

Our model can be extended from two to three spatial dimensions where more crystalline lattice structures become stable [25] and to binary mixtures of driven and undriven particles promising a rich variety of mixed active crystals. In principle, our predictions are verifiable in experiments on self-propelled particles and in particle-resolved computer simulations at high density [13–15]. Very recently, traveling crystals have in fact been found in such simulations [42]. Since the new traveling crystalline structures show a nontrivial dynamical response, they may serve as a building block for a new class of active matter with unusual rheological, phononic, and possibly, also photonic properties.

*menzel@thphy.uni-duesseldorf.de

[1] T. Vicsek, A. Czirók, E. Ben-Jacob, I. Cohen, and O. Shochet, Phys. Rev. Lett. **75**, 1226 (1995).

[2] S. Ramaswamy, Annu. Rev. Condens. Matter Phys. **1**, 323 (2010).

[3] P. Romanczuk, M. Bär, W. Ebeling, B. Lindner, and L. Schimansky-Geier, Eur. Phys. J. Special Topics **202**, 1 (2012).

[4] M. E. Cates, Rep. Prog. Phys. **75**, 042601 (2012).

[5] K. Drescher, J. Dunkel, L. H. Cisneros, S. Ganguly, and R. E. Goldstein, Proc. Natl. Acad. Sci. U.S.A. **108**, 10940 (2011).

[6] W. F. Paxton, K. C. Kistler, C. C. Olmeda, A. Sen, S. K. St. Angelo, Y. Cao, T. E. Mallouk, P. E. Lammert, and V. H. Crespi, J. Am. Chem. Soc. **126**, 13424 (2004).

[7] G. Volpe, I. Buttinoni, D. Vogt, H.-J. Kümmerer, and C. Bechinger, Soft Matter **7**, 8810 (2011).

[8] V. Narayan, S. Ramaswamy, and N. Menon, Science **317**, 105 (2007).

[9] I. Theurkauff, C. Cottin-Bizonne, J. Palacci, C. Ybert, and L. Bocquet, Phys. Rev. Lett. **108**, 268303 (2012).

[10] R. Thar and M. Kühl, Appl. Environ. Microbiol. **68**, 6310 (2002).

[11] R. Thar and M. Kühl, FEMS Microbiol. Lett. **246**, 75 (2005).

[12] G. Grégoire, H. Chaté, and Y. Tu, Physica (Amsterdam) **181D**, 157 (2003).

[13] J. Bialké, T. Speck, and H. Löwen, Phys. Rev. Lett. **108**, 168301 (2012).

[14] G. S. Redner, M. F. Hagan, and A. Baskaran, arXiv:1207.1737.

[15] A. M. Menzel and T. Ohta, Europhys. Lett. **99**, 58001 (2012).

[16] A. Baskaran and M. C. Marchetti, Phys. Rev. Lett. **101**, 268101 (2008).

[17] K. R. Elder, M. Katakowski, M. Haataja, and M. Grant, Phys. Rev. Lett. **88**, 245701 (2002).

[18] J. Toner and Y. Tu, Phys. Rev. Lett. **75**, 4326 (1995).

[19] A. J. Archer and R. Evans, J. Chem. Phys. **121**, 4246 (2004).

[20] H. H. Wensink and H. Löwen, Phys. Rev. E **78**, 031409 (2008).

[21] K. R. Elder and M. Grant, Phys. Rev. E **70**, 051605 (2004).

[22] K. R. Elder, N. Provatas, J. Berry, P. Stefanovic, and M. Grant, Phys. Rev. B **75**, 064107 (2007).

[23] S. van Teeffelen, R. Backofen, A. Voigt, and H. Löwen, Phys. Rev. E **79**, 051404 (2009).

[24] G. Tegze, L. Gránásy, G. I. Tóth, F. Podmaniczky, A. Jaatinen, T. Ala-Nissila, and T. Pusztai, Phys. Rev. Lett. **103**, 035702 (2009).

[25] A. Jaatinen, C. V. Achim, K. R. Elder, and T. Ala-Nissila, Phys. Rev. E **80**, 031602 (2009).

[26] P. Stefanovic, M. Haataja, and N. Provatas, Phys. Rev. Lett. **96**, 225504 (2006).

[27] P. Stefanovic, M. Haataja, and N. Provatas, Phys. Rev. E **80**, 046107 (2009).

[28] P. Y. Chan, G. Tsekenis, J. Dantzig, K. A. Dahmen, and N. Goldenfeld, Phys. Rev. Lett. **105**, 015502 (2010).

[29] J. A. P. Ramos, E. Granato, S. C. Ying, C. V. Achim, K. R. Elder, and T. Ala-Nissila, Phys. Rev. E **81**, 011121 (2010).

[30] G. Tegze, G. I. Tóth, and L. Gránásy, Phys. Rev. Lett. **106**, 195502 (2011).

[31] R. Wittkowski, H. Löwen, and H. R. Brand, Phys. Rev. E **84**, 041708 (2011).

[32] See Supplemental Material at http://link.aps.org/supplemental/10.1103/PhysRevLett.110.055702 for a derivation of the model from a more microscopic dynamical density functional approach and for the consequences of hydrodynamic interactions through a moving background fluid.

[33] R. Wittkowski, H. Löwen, and H. R. Brand, Phys. Rev. E **83**, 061706 (2011).

[34] M. E. Cates and J. Tailleur, arXiv:1206.1805.

[35] J. Toner, Y. Tu, and S. Ramaswamy, Ann. Phys. (N.Y.) **318**, 170 (2005).

[36] J. Tailleur and M. E. Cates, Phys. Rev. Lett. **100**, 218103 (2008).

[37] Y. Fily and M. C. Marchetti, Phys. Rev. Lett. **108**, 235702 (2012).

[38] S. Mishra, A. Baskaran, and M. C. Marchetti, Phys. Rev. E **81**, 061916 (2010).

[39] A. Baskaran and M. C. Marchetti, Phys. Rev. E **77**, 011920 (2008).

[40] H. Tanaka and T. Araki, Phys. Rev. Lett. **85**, 1338 (2000).

[41] J. P. Hernandez-Ortiz, C. G. Stoltz, and M. D. Graham, Phys. Rev. Lett. **95**, 204501 (2005).

[42] E. Frey (private communication).